Bidirectional wakes over complex terrain using SCADA data and wake models

Nanako Sasanuma[1], Akihiro Honda[2], Christian Bak[3], Niels Troldborg[3], Mac Gaunaa[3] and Morten Nielsen[3], Teruhisa Shimada[1]

[1]Graduate School of Science and Technology, Hirosaki University, Bunkyo–cho 3, Hirosaki, 036–8561, Japan
[2]Aomori Public University, Department of Management and Economics, Aomori, Aomori, Japan, 030-0196, Japan
[3]DTU Wind and Energy Systems, Technical University of Denmark, Roskilde, 4000, Denmark

Correspondence to: Nanako Sasanuma (h22ds203@hirosaki–u.ac.jp)

Abstract.

We investigate bidirectional wake effects between the same type of two wind turbines in a hill region in northern Japan using Supervisory Control and Data Acquisition (SCADA) data and validate the simulated wakes by 12 wake models. The extent to which complex terrain affects wake behavior has not yet been fully studied and further understanding of fundamental characteristics of bidirectional wakes over complex terrain is required. The two turbines are located 3.17 times the rotor diameter apart with a different elevation of 0.44 times the rotor diameter. First, we identify the wake effects in terms of wind speed ratio, which is defined as a ratio of wind speed at the downstream wind turbine to that at the upstream wind turbine. By comparing the conditions according to the operating state of the upstream wind turbine, the wakes are clearly detected as minimum wind speed ratios for northeasterly and southwesterly winds. The wind speed ratio decreases with inflow wind speed below the rated wind speed. Increase in turbulence intensity and decrease in power output are greater for southwesterly wind than for northeasterly wind. This difference arises from the combined effects of the turbine-induced wake and the terrain-induced variation in wind speed. Then, we examine the winds and wind turbine wakes over complex terrain by using Wind Atlas Analysis and Application Program Computational Fluid Dynamics (WAsP CFD) in combination with PyWake. The wind speed ratios derived from the wake models show strong dependence on inflow wind speed, reflecting the thrust curve used in the wake models. The wake models commonly overestimate the reduction in wind speed for northeasterly wind and underestimate it for southwesterly wind. This comparative study contributes to understanding the additional effects of topography on wake effects in onshore wind power plants and offshore wind power plants near the coast.

1 Introduction

Considering effects of wake generated by neighbouring wind turbines is crucial to design a layout of wind power plant. We need to manage the wake effects, and otherwise, wakes can negatively impact downstream wind turbines by reducing wind speeds and power output and by increasing turbulence intensity and resulting higher load fluctuation. Moreover, complex terrain, the topography affects the wakes and makes the airflow more complex. An increasing number of wind turbines are being installed in complex terrains, such as hills, escarpments, valleys, and gorges, with decreasing in flat terrain suitable for wind power plants. Although installation in complex terrain poses logistic challenges, strong winds induced by topographic effects offer an advantage for wind resource (e.g., Yamaguchi et al., 2024). Thus, the combined effects of wake and terrain further complicate the optimization of the performance and control strategies of wind power plants.

Analyzing wind measurement data is essential for understanding wake phenomena (e.g., Rhodes and Lundquist, 2013; Hansen et al., 2016; El-Asha et al., 2017; Mittelmeier et al., 2017; Astolfi et al., 2018; Han et al., 2018). Among observational data, supervisory control and data acquisition (SCADA) provides an advantage on concurrent analysis of the actual conditions of wind at the hub height and operating states of wind turbines. In addition to the SCADA data, external measurements, such as light detection and ranging (LiDAR) measurements, are widely used to observe wakes. Combined use of various observations enables to further

investigate the impact of wakes on power generation of downstream wind turbines in flat terrain (El-Asha et al., 2017) and in complex terrain (Han et al., 2018), and on turbulence intensity of downstream wind turbines (Mittelmeier et al., 2017). Rhodes and Lundquist (2013) indicate dependence of wake effects on inflow wind speed and the vertical structures of reduction in wind speed and of increase in turbulence intensity due to wake by installing two doppler lidars for upstream and downstream wind turbines. Astolfi et al. (2018) use SCADA data with numerical simulation to demonstrate that the wake structures are distorted by the surrounding terrain and that wind speed recovery is quicker over complex terrain than over flat terrain. Using SCADA data in conjunction with external equipment is an effective method for wake detection. However, using external equipment involves high costs for operation and maintenance, and operation periods of the external equipment are often limited.

Numerical simulations enable to effectively analyse the wake and complement observations (Göçmen et al., 2016; Carbajo Fuertes et al., 2018; Bastankhah and Porté-Agel, 2014; Fischereit et al. 2022; Troldborg et al., 2022). Göçmen et al. (2016) suggest that wake models have different advantages in terms of usability, accuracy, quantity and quality of input data, and computational costs by evaluating utilization of the six wake models with SCADA data in onshore and offshore wind power plants. Gaussian wake model is validated by two pulsed scanning Doppler lidars mounted on the nacelle, which measure both the incoming flow and the downstream wake (Carbajo Fuertes et al., 2018). Bastankhah and Porté-Agel (2014) validate a Gaussian model for the reproducibility of wind speed at the downstream wind turbine by wind-tunnel measurements and the large-eddy simulations (LES). Fischereit et al. (2022) indicate that the selected wake models accurately represent intra-farm wakes; however, they underestimate the farm-farm wake effects compared with high-fidelity simulations. Troldborg et al. (2022) found that the performance of wind turbines in complex terrain is highly variable compared to that in flat homogeneous terrain by using LES. Wake models have been validated by various methods; however, a limited number of studies have validated simulated wakes over the complex terrain.

The following studies have investigated fundamental behaviour of wakes over complex terrain all over the world. Porté-Agel et al. (2020) mention that the combined study of wind turbine wakes and topography has still much room to development. The measurement campaign in a double-ridge site using the meteorological measurement in Perdigão field in 2017 is well-known observational field experiment over a complex terrain (Wagner et al., 2019). The wake generated by a single wind turbine at the ridge goes up because a strong recirculation zone is creased in a downstream (e.g., Berg et al., 2017; Dar et al., 2019; Wenz et al., 2022). Letzgus et al. (2022) demonstrate that high turbulence flow due to the topography results in asymmetric torque distributions and leads to increased load fluctuations of a wind turbine in a flat plateau downstream of escarpment by using numerical simulation. However, simulation of wind in complex wind is still a challenge (Castellani et al., 2015) and lack of clarity about inflow wind speed in complex terrain (Politis et al., 2011). Yang et al. (2015) show the decrease in wind speed and increase in turbulence intensity induced by the upstream trench of by using several hypothetical wind turbines. Fleming et al. (2019, 2020) demonstrate a 14% increasing in energy production with wake steering for an upstream-downstream wind turbine pair in complex terrain. Sasanuma and Honda (2022; 2024) focus on two onshore wind turbines in complex terrain in northern Japan (Fig. 1) and investigated the wake effects of one turbine on the other. The southwesterly winds result in significant reduction in wind speed and an increase of turbulence intensity at the downstream wind turbine (Sasanuma and Honda, 2022). Sasanuma and Honda (2024) indicate that wake models generally underestimate the reduction in wind speed in the wakes compared with those observations. Currently, the suitable sites for investigating of the fundamental bidirectional wake behavior between two wind turbines are few.

However, we need to further explore the wakes between two wind turbines for evaluating wake effects induced by multiple upstream of wind turbines or by wind power plants. First, we need to compare bidirectional wake effects between the two wind turbines to clarify the differences in wake effects over the complex terrain according to the wind direction. Sasanuma and Honda (2022; 2024) investigate wake effects only one-way direction between the two turbines. Wake effects in the other direction remain unclear. Moreover, we need to look into the dependence of wake effects on inflow wind speed over complex terrain. Second, we need to validate the performance of the wake models by comparing the simulated results with the observed results by the SCADA data and to clarify the dependence of simulated wake effects on inflow wind speed. The validation of wakes over complex terrain

is still insufficient. By comparing the mutual wake effects between wake models, we need to identify similarities and differences among the wake models.

We statistically investigate the bidirectional wakes behavior between two wind turbines over the complex terrain using the SCADA data and validate the performance of wake models in terms of reduction in wind speed at the downstream wind turbine by comparing with the SCADA data. We specifically address the following two issues: (1) to identify the wake effects at the downstream wind turbine by comparing the conditions with and without the operation of the upstream wind turbine and evaluate the wake effects in terms of reduction in wind speed, turbulence intensity, and power output. (2) to demonstrate the difference in reproducibility of mutual wakes between two wind turbines simulated by 12 wake models. Note that we used the default values of the 12 wake models without adjusting the parameters to get closer to the results of the SCADA data. The sensitivity analysis is beyond the scope of this study. This research highlights the effectiveness of using the SCADA data to investigate flow characteristics arising from both surrounding topography and wakes created by upstream wind turbines. Moreover, we demonstrate the potential to utilize the SCADA data and to derive wake information.

Section 2 describes the wind turbines, the SCADA data, the wind condition at the site, the methodology to detect of wake effects, and the flow simulation with wakes. Section 3 analyses the SCADA data to examine the wake effects and compares the observed results with the simulated results by wake models. Section 4 presents the summary and conclusions.

2 Data and Methodology

2.1 Study site and two wind turbines

This study focuses on two wind turbines (WT1 and WT2) located near the northern tip of the Tsugaru Peninsula, Japan (Fig. 1). Because the region near Cape Tappi is characterized by abundant wind resources and steep topography, this site has been a research site for operation of wind turbines since the first utility-scale wind farm in Japan was built in 1991 (Fig. 1; e.g., Ushiyama, 1999; Inomata et al., 1999; Enomoto et al., 2001; Fujikawa et al., 2002; Hasegawa et al., 2003). The original model of the two wind turbines is J82-2.0 manufactured by Japan Steel Works with a hub height of 65.0 m and a rotor diameter of 83.3 m (Fig. 2a). Rated power output is 1.675 MW. Full operation started in 2010. The two wind turbines are located almost in a southwest-northeast direction (Fig. 1) and the horizontal distance between the two turbines is 3.17 times the rotor diameter (264 m; Fig. 2b). WT1 and WT2 are located at an altitude of 132 m and 169 m, respectively. The difference in elevation correspond to 0.44 times the rotor diameter. Along the line connecting the two turbines, WT2 is located at the highest location (Fig. 2b). The surrounding terrain is covered by bush trees (Fig. 2a).
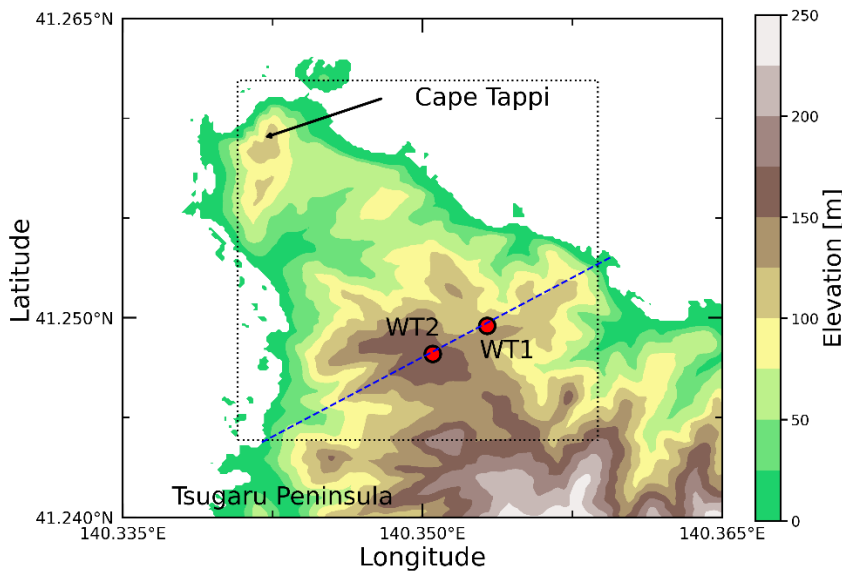
110

Figure 1. The topography of the study site (color shading) and the locations of the two wind turbines (WT1 and WT2; red circles). The blue dashed line represents the line connecting the two wind turbines to show the vertical topography in Fig. 2b and to analyze the vertical cross section in Fig. 14. The square enclosed by the dotted line is a 2 km × 2 km computational domain for WAsP CFD.
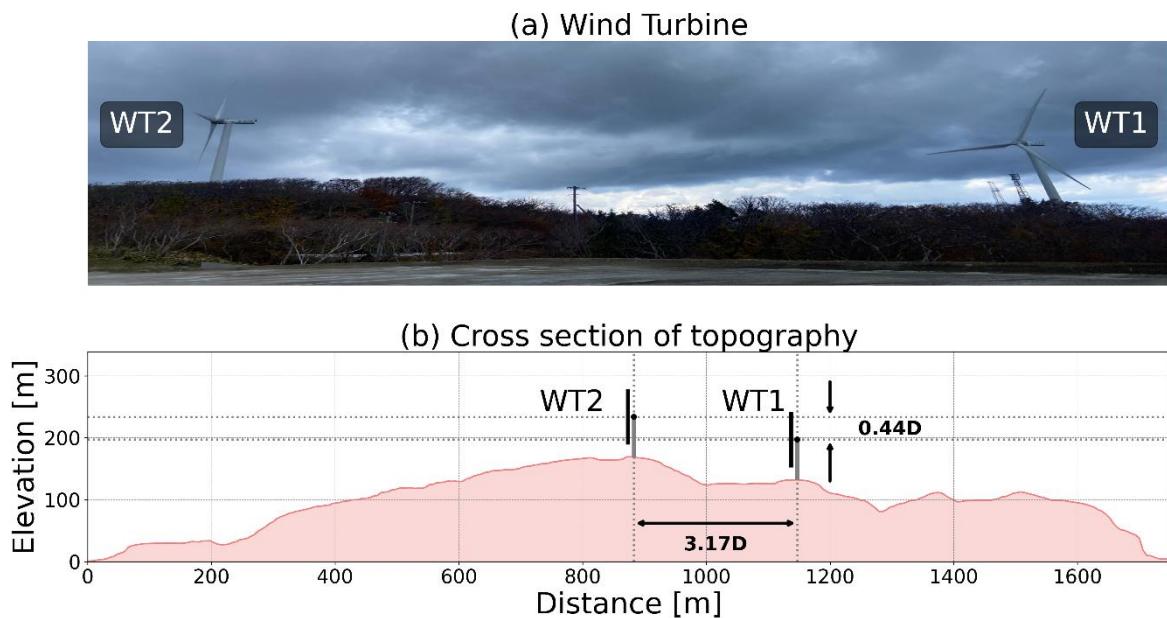
115

Figure. 2 (a) Photo of the two wind turbines. (b) Cross section of the topography along the line connecting the two wind turbines shown in Fig. 1. The elevation data are obtained from the website of Geospatial Information Authority of Japan (Geospatial Information Authority of Japan, 2025).

2.2 SCADA data at the two wind turbines

120 We used 10-minute mean SCADA data of the two wind turbines from 5 September 2015 to 31 December 2017. The original data are sampled at an interval of 1 second. The dataset includes wind speed, wind direction, standard deviation of wind speed, nacelle direction, blade pitch angle, rotor speed, and power output. The wind data are measured by a wind vane and a three-cup type

anemometer mounted at the rear of the nacelle. Turbulence intensity is defined as σ/WS, where σ is standard deviation of wind speed, and WS is the 10-minute mean wind speed. To effectively investigate the dependency of the wind turbine wake on wind direction, we used the data with the yaw misalignment, a difference between wind direction and nacelle direction, within plus or minus 10°. A total of 80% of the data satisfy this condition. In the following analyses, we used the SCADA data after applying this selection based on yaw misalignment.

2.3 Wind climate

We present the wind climate at the two wind turbines from the SCADA data (Figs. 3 and 4). The westerly wind and easterly wind commonly dominate at WT1 and WT2 (Fig. 3). Strong westerly winds dominate in winter due to the Siberian high, whereas easterly winds intermittently blow in summer due to the Okhotsk high (Shimada et al., 2014). Westerly winds are stronger than easterly wind and the wind direction from southwest to west-northwest account for 51% at WT2 (Fig. 3a) and 52% at WT1 (Fig. 3b). Both wind turbines have abundant wind resources with annual mean wind speed above 8 m s^{-1} (Figs. 3a and 3b). WT2 exhibits higher speeds than WT1 because WT2 is located on top of the hill and wind is accelerated on the hill (Yamaguchi et al., 2002). The frequency exceeding 15 m s^{-1} amount to 5% at WT1 and 14% at WT2 in all wind direction. The overall results are consistent with the results without data selection based on yaw misalignment (Fig. 3, Sasanuma and Honda, 2022 and Sasanuma and Honda, 2024). The wind speeds at WT1 and WT2 show significant correlation (Fig. 4a). Wind speeds at WT2 show 20% higher than those at WT1. Wind directions at WT1 and WT2 are in good agreement (Fig. 4b). The data are concentrated in the easterly wind (90°–100°) and the westerly wind (220°–260°), which is consistent with Fig. 3. This means that the dominant wind blows almost along the line connecting the two turbines and that the locations of the two wind turbines are suitable for analysing mutual wake effects between the wind turbines.
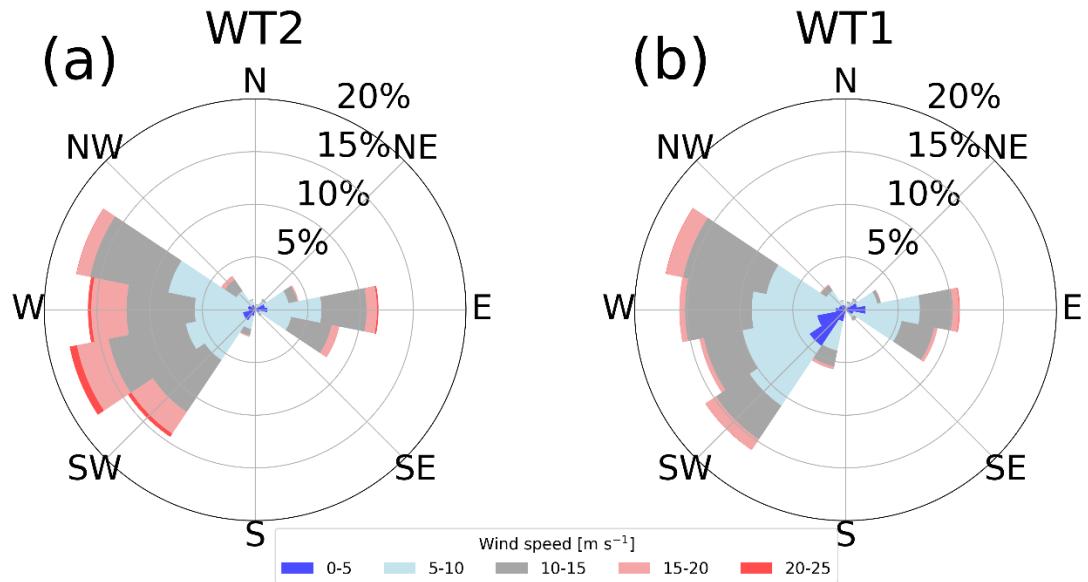
Figure 3. Wind roses derived from the SCADA data of (a) WT2 and (b) WT1. The frequencies are shown at every 5 m s⁻¹ with different colors. Wind direction is defined as the direction from which the wind blows.
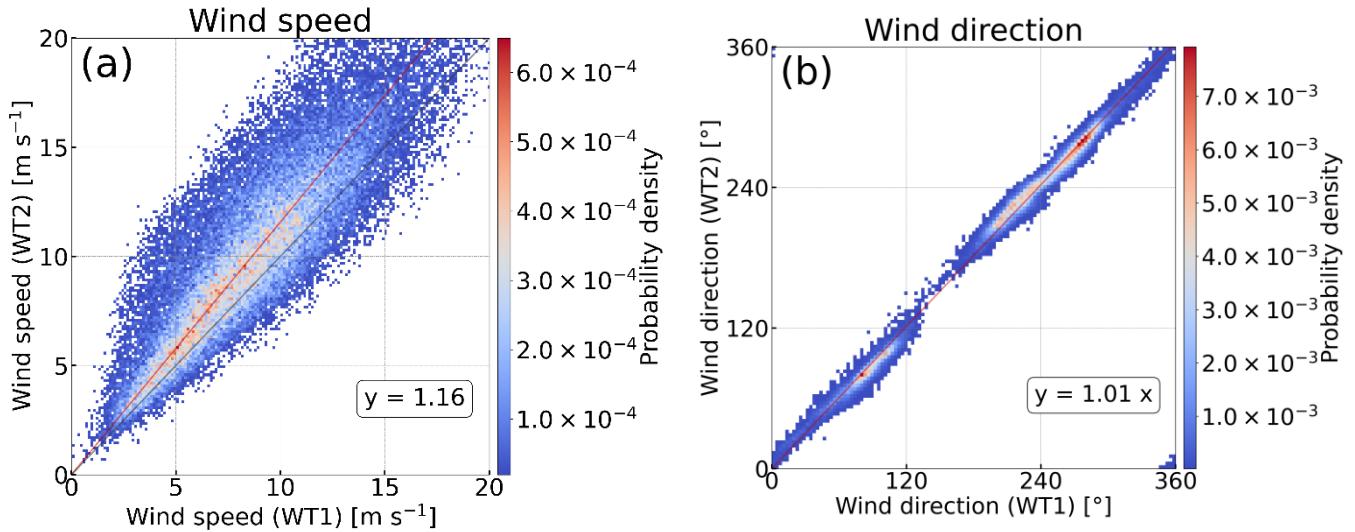
Figure 4. Scatter plots of (a) wind speed and (b) wind direction between WT1 and WT2 from the SCADA data. The color represents the data density. The red lines in (a) and (b) are the linear regression lines, shown by the equation in the figures. The black line in (a) represents a 1:1 line.

2.4 Detection of wake effects

To assess the wake effects generated by the upstream wind turbines only based on the SCADA data, we divided the data into two categories on the basis of the operating state of the upstream wind turbine: "no-wake conditions" and "wake conditions" (Sasanuma and Honda, 2022; Sasanuma and Honda, 2024). "No-wake conditions" mean that the upstream wind turbine is not operating and "wake conditions" mean that the upstream wind turbine is in operation. Sasanuma and Honda (2024) identified the operating states of wind turbines by a combination of rotor speed, blade pitch angle, and power output. We found that we can distinguish whether the turbine is operating or not only by the blade pitch angle. By imposing the condition that the blade pitch angle is within ±3°, we can extract the data when the wind turbine is in operation below the rated wind speed. The blade pitch angle is 90° when the wind turbine is not operating. When considering wake conditions, we focus on the data with wind speeds ranging from the cut-in wind speed and the rated wind speed. In this range, wake effects are maximized, and, above the rated wind speed, wake effects are reduced

by the blade pitch control (e.g., El-Asha et al., 2017; Dilip and Porté-Agel, 2017; Duncan et al., 2020). Thus, by comparing no-wake conditions and wake conditions, we can statistically analyse the influence of wakes generated by the upstream wind turbine on mean wind speed, turbulence intensity, and power output at the downstream wind turbine.

2.5 Wind speed ratios

To analyse mutual wake effects between the two wind turbines, we define a wind speed ratio of wind speed at the downstream wind turbine to that at the upstream wind turbine. We should notice that the definition of the wind speed ratio between wind speed at WT1 (WS_1) and that at WT2 (WS_2) differs by wind direction. When northeasterly wind blows, wakes induced by WT1 influence WT2. Thus, the wind speed ratio is defined as WS_2 / WS_1. When southwesterly wind blows, wakes induced by WT2 influence WT1. Thus, the wind speed ratio is defined as WS_1 / WS_2. We summarize the wind speed ratios in no-wake conditions and in wake conditions for the respective northeasterly wind and southwesterly wind in Table 1. We compare the wind speed ratio between no-wake and wake conditions and between northeasterly wind and southwesterly wind to evaluate the wake effects in following analysis.

Table 1. Definition of wind speed ratio according to the combination of the presence or absence of wake and wind directions. White shading indicates the condition that the upstream wind turbine is not in operation, and gray shading indicates the condition that the upstream wind turbine is in operation.

	Northeasterly wind	Southwesterly wind
No-wake conditions	WS_2 / WS_1	WS_1 / WS_2
Wake conditions	WS_2 / WS_1	WS_1 / WS_2

2.6 Flow simulations with wake models

We utilized Wind Atlas Analysis and Application Program Computational Fluid Dynamics (WAsP CFD; Bechmann, 2012) in combination with PyWake (Pedersen et al., 2023) to closely examine the observed wind and wakes over complex terrain. WAsP CFD is a CFD model integrated into WAsP and is designed for simulating winds over complex terrain. The model is based on Ellipsys 3D code, which is a multiblock finite volume discretization of incompressible Reynolds Averaged Navier-Stokes (RANS) equations. Simulations are conducted under the assumption of a neutral atmospheric stability. Cariolis forcing is neglected. The validity of WAsP CFD in complex terrain has been demonstrated (e.g., Bechmann et al., 2011; Troen et al., 2015; Bechmann, 2016; Sharma et al., 2020). We used WAsP CFD for evaluating the influence of topography on wind flow. Computational domain is shown in Fig. 1. The horizontal grid interval is 90 m and the elevation map used is spaced at 5 m intervals (Geospatial Information Authority of Japan, 2025). The data are output at 13 levels from 5 m to 300 m (5, 10, 20, 33, 48, 65, 80, 100, 120, 150, 200, 250, and 300 m) from the ground level. The upper boundary of the computational domain is 7000 m. We set the inflow wind speed for far upwind. In this case, the wind speed is 10 m s^{-1} at 100 m height and roughness length is 0.0032 m. Therefore, the inflow wind speed has a slightly sheared profile. WAsP CFD uses the roughness length depending on landscape type. The roughness length in the study area ranges from 0.1 to 1.0 m.

PyWake is an open-source wind farm simulation tool written in Python. This tool simulates the flow with wind turbines by incorporating wake models. PyWake has 12 wake models (Appendix A): 11 engineering wake models and a linearized RANS wake model (Fuga). Bastankhah model and TurboGaussian model have the same wind deficit model defined with a Gaussian profile (Bastankhah and Porté-Agel, 2014; Pedersen et al., 2022). They have been validated for onshore field (e.g., Jeon et al., 2015; Ruisi et al., 2019; Fleming et al., 2020; zum Berge et al., 2024) and offshore filed (Farrell et al., 2021; Fischereit et al., 2022; Centurelli

et al., 2024). The turbulence intensity in PyWake uses is 0.2. We used the thrust curve of the V80 2MW wind turbine because the rated power output of this wind turbine is closest to that of the wind turbines in this study among the wind turbine models available in PyWake. The thrust curve of the V80 is shown in Fig. 5. In this study, we discuss similarities and differences between the wake models for mutual wind directions when a typical thrust curve is used.
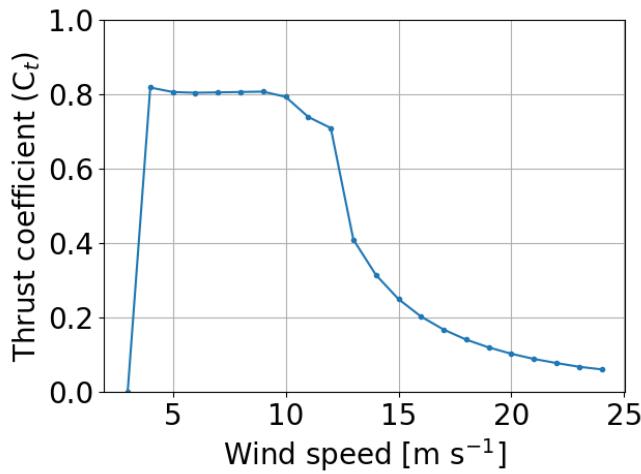
Figure 5. Thrust coefficient as a function of wind speed from V80 wind turbine.

3 Results

3.1 Observational results

We examine the wind speed ratios to evaluate wake effects caused by the upstream wind turbine. Figure 6 shows wind speed ratios between the two wind turbines before we divided the data into two categories on the basis of the operating state of the upstream wind turbine. The wind speed ratios are generally above 1.0 in Fig. 6a and below 1.0 in Fig. 6b, whereas we can identify V-shaped curves or significant reductions in wind speed ratio at around 40° and 225° (light blue shading in Figs. 6a and 6b). The ranges of these significant reductions are approximately ±10° on both sides of the wind directions. We can see no other significant reduction in other wind direction ranges. The wind directions of 45° and 225° nearly correspond to the direction of the line connecting the two wind turbines located in the northeast-southwest direction (Fig. 1). Thus, mutual wakes between the two wind turbines cause the significant reductions in wind speed ratio. We focus on the wind directions of 45° and 225° in the following analyses.
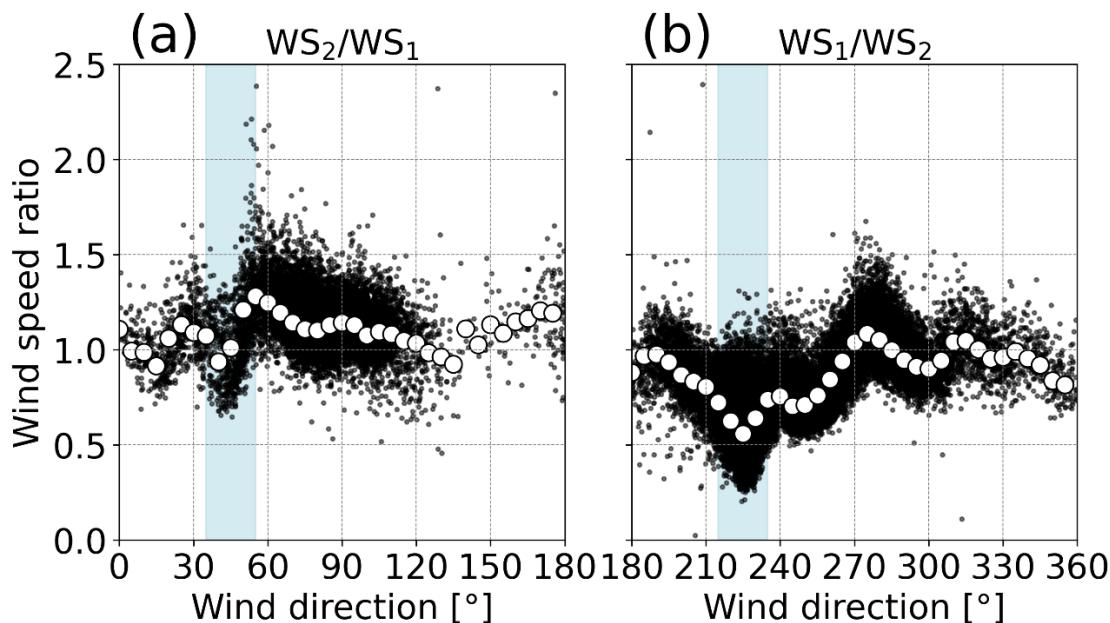
Figure 6. Wind speed ratios as a function of wind direction. Black dots denote 10-minute mean data and white circles denote median values in every 5º bin. In (a) and (b), wind directions at WT2 are used for the horizontal axes. Note that the definition of the wind speed ratio differs between (a) and (b). In (a), wind speed ratio is defined as the ratio of wind speed at wind turbine 2 (WS_2) to that at wind turbine 1 (WS_1). In (b), wind speed ratio is defined as the ratio of WS_1 to WS_2. These definitions of the wind speed ratio are common in the following analyses. Light blue shading indicates the ranges of wind direction with wake effects for (a) 45º±10º and (b) 225º±10º.

To clearly elucidate wake effects from the results of Fig. 6, we divide the data by the operating state of the upstream wind turbine. The condition of blade pitch angle is applied, and resultantly the data with higher than the rated wind speed is excluded. We compare the wind speed ratio between no-wake conditions and wake conditions with a focus on the V-shaped curve at around 45°±10° and 225°±10° (Fig. 7). For northeasterly wind, the plots show no V-shaped curve and remain generally constant in no-wake conditions (Fig. 7a). The wind speed ratios are higher than 1.0 with a median value of 1.18 at 45° and this means that the wind speeds at WT2 are higher than those at WT1. In wake conditions, we can see a significant reduction in wind speed ratio due to the wake of WT1 with a maximum reduction of 23% at wind direction of 45° (Fig. 7b). For southwesterly wind, as is the case with Fig. 7a, the plots show no V-shaped curve and have almost the constant wind speed ratio in no-wake conditions (Fig. 7c). The median value of wind speed ratio is 0.87 at 225°. The wind decelerates from the location of WT2 to the location of WT1 even without wakes generated by WT2 because WT1 is positioned behind the hill. In wake conditions, wind speed ratio decreases to 0.47 from 0.87 in no-wake condition and this means with a 46% reduction at 225° (Fig. 7d). This reduction observed for southwesterly wind is greater than that observed for northeasterly winds. This reduction is 22% larger than those derived by Sasanuma and Honda (2022) because they use the mean values and not the median values. From the above results, we find that the operation of the upstream wind turbine causes wind speed reduction at the downstream wind turbine and that the wake effect on the downhill side for southwesterly wind is more pronounced than that on the uphill side for northeasterly wind.
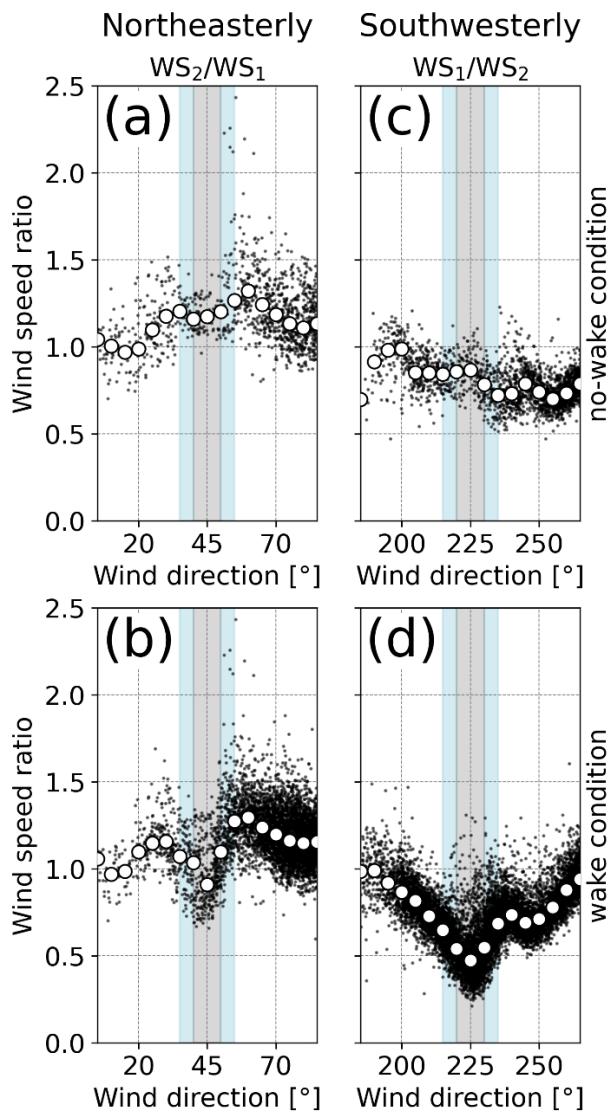
240

Figure 7. The same as in Fig. 6 but for being classified by the operating state of the upstream wind turbine in (a) (c) no-wake conditions and (b) (d) wake conditions for (a) (b) northeasterly wind and (c) (d) southwesterly wind. Light blue and gray shadings indicate the range of wind direction with wake effects. The gray shading in the ranges of (a) (c) 45°±5° and (b) (d) 225°±5° represent the targeted ranges of wind direction for the analyses in Figs. 8, 9 and 10.

245

We examine the dependence of the magnitude of reduction in wind speed on inflow wind speed in wake conditions (Fig. 8). To examine the maximum wake effects, we focus on the ranges of wind direction for 45°±5° and 225°±5° (gray shading in Fig. 7). We use the wind speed of the upstream wind turbine for inflow wind speed and for the horizontal axis when the upstream wind turbine is in operation. Figure 8 clearly shows the relationship between inflow wind speed and wind speed ratio for both northeasterly and

250 southwesterly winds. The decrease in wind speed ratio means the increase in wake effect or the large reduction in wind speed at the downstream wind turbine. For northeasterly wind, the wind speed ratio decreases as the inflow wind speed increases below a wind speed of 6 m s^{-1}, whereas, above 6 m s^{-1}, the wind speed ratio remains almost constant (Fig. 8a). For southwesterly wind, the wind speed ratio decreases with inflow wind speed and reach a minimum at 10 m s^{-1} (Fig. 8b). The gradual increase above 10 m s^{-1} suggests a start of control of the blade pitch angle. Thus, the wind turbine extracts the kinetic energy from the wind below the rated

255 wind speed and the resulting momentum loss in the downstream induce the maximum wake effects. These results are consistent with those of Rhodes and Lundquist (2013) showing that the maximum reduction in wind speed occurs below the rated wind speed.
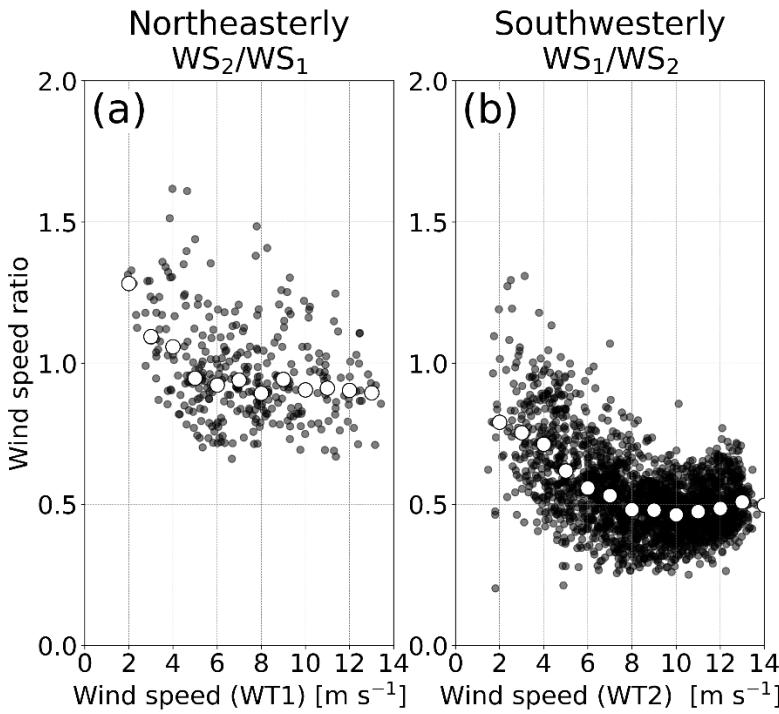
Figure 8. Wind speed ratio as a function of wind speed at the upstream wind turbine for (a) northeasterly wind and (b) southwesterly wind. Black dots denote 10-minute mean data and white circles denote median values in every 1 m s^{-1} bin.

We investigate the wake effects on the turbulence intensity at the downstream wind turbine by comparing the observed turbulence intensity with the standard curves of turbulence intensity defined by the International Electrotechnical Commission (IEC, 2019). Two categories of the standard curves are given by the following equations. WS is wind speed.

$$\text{Turbulence instensity}_{\text{category}}A = 0.16\,(0.75 + 5.6\,/\,WS) \tag{1}$$
$$\text{Turbulence instensity}_{\text{category}}A^+ = 0.18\,(0.75 + 5.6\,/\,WS) \tag{2}$$

For northeasterly wind, the 90th percentile values of turbulence intensity hardly exceed the line of A+ category commonly in no-wake conditions and wake conditions (Figs. 9a and 9b). The wakes generated by WT1 contribute little to the increase in turbulence intensity at WT2. For southwesterly wind, the 90th percentile values of turbulence intensity for wind speeds greater than 7 m s^{-1} follows the line of A+ category in no-wake conditions (Fig. 9c). In wake conditions, wind speed at WT1 decreases to less than 10 m s^{-1} due to the wake generated by WT2 and the 90th percentile values of turbulence intensity follow the lines of A+ category and A category (Fig. 9d). However, the 10-minute mean data of turbulence intensity above the 90th percentile significantly exceeds the line of A+ category. The 10-minute mean data of turbulence intensity exceed 0.4 for wind speed less than 6 m s^{-1}. This is a noticeable difference between no-wake conditions and wake conditions. The wakes generated by WT2 cause high turbulence intensity at WT1 when the southwesterly wind blows (Sasanuma and Honda, 2022). These results suggest that the wake effects on the turbulence intensity significantly vary depending on the topography.
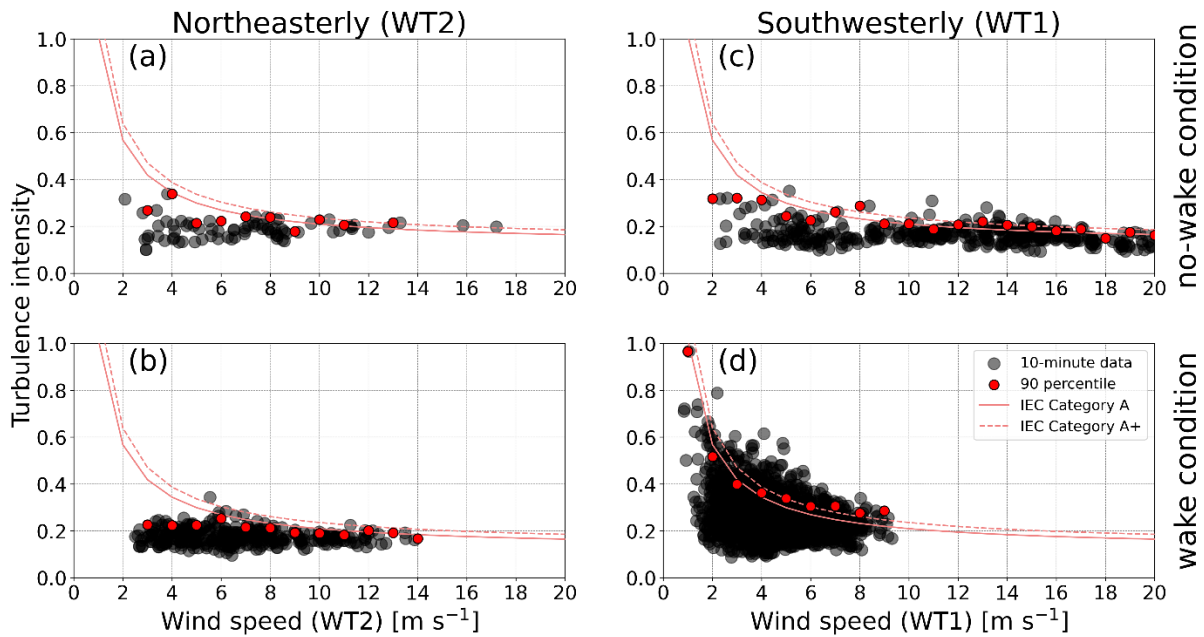
Figure 9. Turbulence intensity as a function of wind speed at the downstream wind turbine in (a) (c) no-wake conditions and (b) (d) wake conditions for (a) (b) northeasterly wind and (c) (d) southwesterly wind. The data are extracted from the focused range of wind direction, denoted by the gray shading in Fig. 7. The horizontal axis represents wind speed at the downstream wind turbine, WT2 in (a) and (b), and WT1 in (c) and (d). Black dots denote 10-minute mean data, and red circles denote 90th percentile values in every 1 m s⁻¹ bin. The red dashed lines indicate standard curves of International Electrotechnical Commission (IEC) category A for very high turbulence by equation (1), and the red solid lines indicate standard curves of IEC category A+ for high turbulence by equation (2).

The impact of the wake on the power output of the downstream wind turbine is examined within the ranges of wind direction of 45°±5° and 225°±5° (Fig. 10). Note that the horizontal axis in Fig. 10 represents wind speed at the upstream wind turbine to examine the reduced power output at the downstream wind turbine compared with the power output at the upstream wind turbine. For northeasterly wind, the power output at the downstream wind turbine, WT2 is lower than that expected from the wind speed at the upstream wind turbine, WT1 (Figs. 10a and 10b). For example, in no-wake conditions, the normalized power output is approximately 0.5 at a wind speed of 8 m s⁻¹ (Fig. 10a). In wake conditions, a wind speed of 9 m s⁻¹ or a 12.5% increase in wind speed at the downstream wind turbine is required to generate the same power output (Fig. 10b). For southwesterly winds, the power output at the downstream wind turbine WT1 decreases more significantly than that expected from the wind speed at the upstream wind turbine, WT2 (Figs. 10c and 10d). For instance, the normalized power output is approximately 0.2 at 7 m s⁻¹ in no-wake conditions (Fig. 10c). In wake conditions, a wind speed of 12 m s⁻¹ or a 71% increase in wind speed is required to generate the same power output (Fig. 10d). At 14 m s⁻¹, the normalized power output in no-wake conditions is approximately 0.9 (Fig. 10c), whereas it decreases to approximately 0.3 in wake conditions (Fig. 10d). This result represents a 67% reduction in power output in case that we assume the same inflow wind speed at the downstream wind turbine with that at the upstream wind turbine. These findings suggest that the wake effects have a more pronounced impact on power output for southwesterly wind than northeasterly wind. Even when the same wind speed is observed at the upstream wind turbine, the degree of reduction in wind speed or the resulting power output at the downstream wind turbine is different depending on the installation conditions of wind turbines.
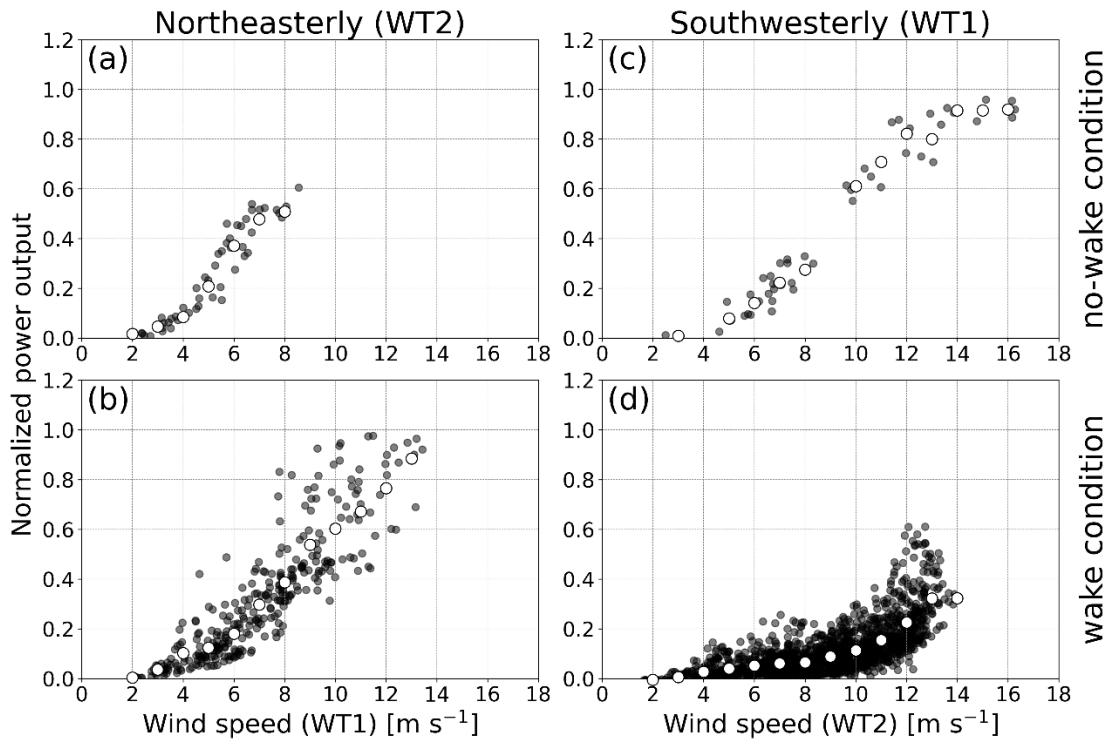
Figure 10. Normalized power output as a function of wind speed at the upstream wind turbine in (a) (c) no-wake conditions and (b) (d) wake conditions for (a) (b) northeasterly wind and (c) (d) southwesterly wind. The normalized power output in the vertical axis represents power output divided by the rated power output. The horizontal axis represents wind speed at the upstream wind turbine, WT1 in (a) and (b), and WT2 in (c) and (d). Black dots denote 10-minute mean data, and white circles denote median values in every 1 m s^{-1} bin. The data are extracted from the focused range of wind direction, denoted by the gray shading in Fig. 7.

3.2 Simulated wake and wind flow

We validate the performance of 12 wake models in PyWake by comparing the wind speed ratios computed from the wake models with those from the SCADA data. We show the comparison results of wind speed ratio for different inflow wind speeds computed by WAsP CFD and a typical wake model, TurboGaussian wake model for northeasterly and southwesterly winds (Fig. 11). The wind speed ratio decreases significantly with decrease in inflow wind speed in the ranges of wind direction with wake effects for both northeasterly winds and southwesterly winds. This means that significant reduction in wind speed occurs when inflow wind speed is small. The magnitudes of reduction in wind speed ratio are the same for wind speeds below 9 m s^{-1} for northeasterly wind (Fig. 11a) and below 8 m s^{-1} for southwesterly wind (Fig. 11b), resulting from the thrust curve used for the wake model (Fig. 5). The wake model shows the results close to those from the SCADA data at inflow wind speed of 13 m s^{-1} for northeasterly wind and at inflow wind speed less than 8 m s^{-1} for southwesterly wind. The model results overestimate the reduction in wind speed for northeasterly wind and underestimate it for southwesterly wind, which is roughly consistent with the results of other wake models (Figs. B1 and B2). All the wake models except the GCL wake model overestimate the reduction in wind speed for northeasterly wind. Most of the results underestimate the reduction in wind speed for the southwesterly wind except Bastankhah and Turbo Gaussian wake models. We can conclude that the topographic effects cause an opposite change in wake reproduction.
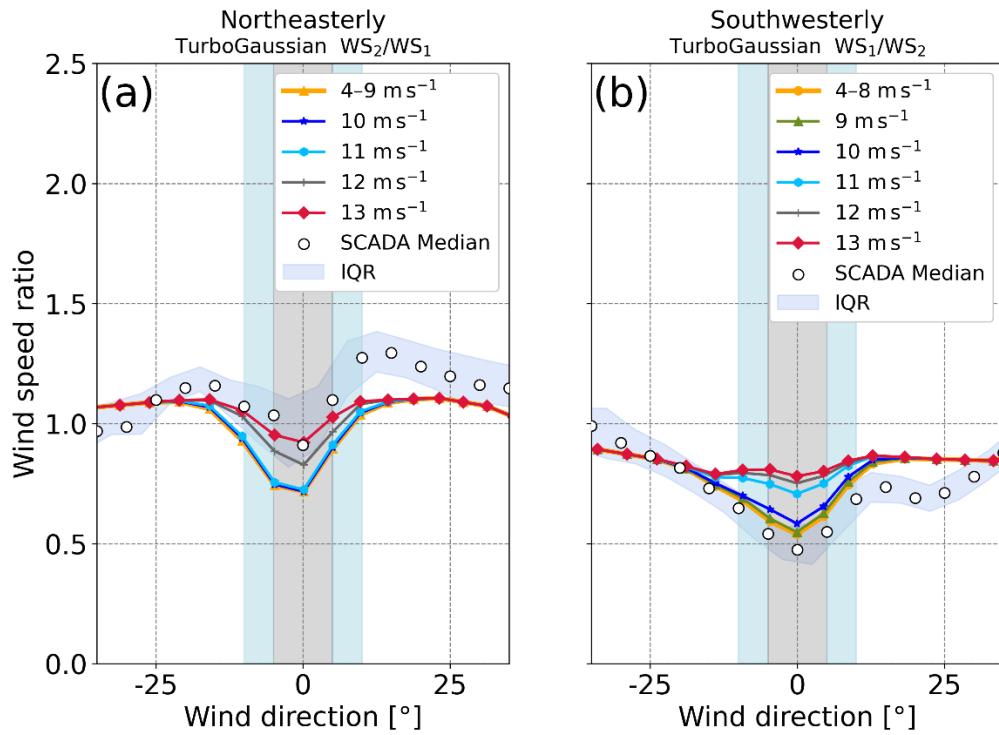
Figure 11. Wind speed ratio as a function of wind direction for (a) northeasterly wind and (b) southwesterly wind. ==The horizontal axis indicates differences in wind direction with the minimum wind speed ratio at 0º for both the SCADA data and the results of the wake models.== The blue band denotes ==the interquartile range (IQR)== of the SCADA data and white circles denote median values in every 5º bin. Colored lines are results derived from TurboGaussian ==wake model== for every 1 m s^{-1} ==inflow wind speed== for 4–13 m s^{-1}. The results for (a) 4–9 m s^{-1} and (b) 4–8 m s^{-1} are shown by one line because the differences are negligible. Light blue and gray shadings indicate the ranges of wind direction with wake effects.

We compare the wind speed ratio derived from the 12 wake models at the inflow wind speeds at ==13 m s^{-1}== for northeasterly wind and ==8 m s^{-1}== for southwesterly wind (Fig. 12). ==For both northeasterly wind and southwesterly wind, most of the wake models underestimate the reduction in wind speed and represent weak wakes (Figs. 12a and 12b).== For ==northeasterly wind, most of the wake models hardly represent the wakes (Fig 12a), for== southwesterly wind, all the wake models except GCL wake model represent a reduction of wind speed ratio (Fig 12b). Only Bastankhah and Turbo Gaussian wake models closely represent the minimum value of wind speed ratio derived from the SCADA data ==at wind directions with a maximum reduction in wind speed for both northeasterly wind and southwesterly wind.== To summarize the validation results from each wake model, we show the wind speed ratio for 12 wake models ==at wind directions with a maximum reduction in wind speed for both northeasterly and southwesterly winds== in Fig. 13. The order of the wake models according to the difference of the results between each wake model and the SCADA data are almost the same for northeasterly and southwesterly winds (Figs. 13a and 13b). The results from Turbo Gaussian and Bastankhah wake models agree with those from the SCADA data and Blondel2020 and Blondel2023 wake models follow the two wake models commonly for northeasterly and southwesterly ==winds.== The differences from the SCADA data ranges from ==0.12% to 17%== for northeasterly wind and from ==6.7% to 68%== for southwesterly wind. The differences between the wake models are more prominent for southwesterly wind than for northeasterly wind. We need to pay attention to the accuracy of the reproduction and the choice of the wake models, as well as topographic situations.
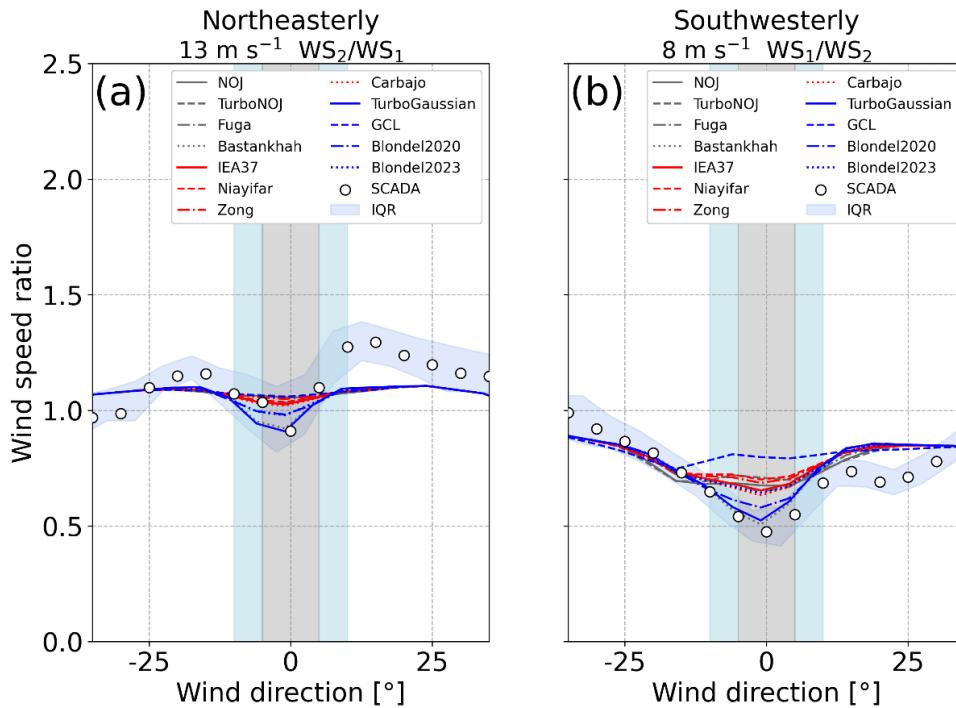
355

Figure 12. Wind speed ratio as a function of wind direction for (a) northeasterly wind and (b) southwesterly wind. The horizontal axis indicates differences in wind direction with the minimum wind speed ratio at 0º for both the SCADA data and the results of the wake models. The blue band denotes the interquartile range (IQR) of the SCADA data and white circles denote median values in every 5º bin. Colored lines are results derived from 12 wake models at inflow wind speed of (a) 13 m s^{-1} and (b) 8 m s^{-1}. Light blue

360 and gray shadings indicate the ranges of wind direction with wake effects.
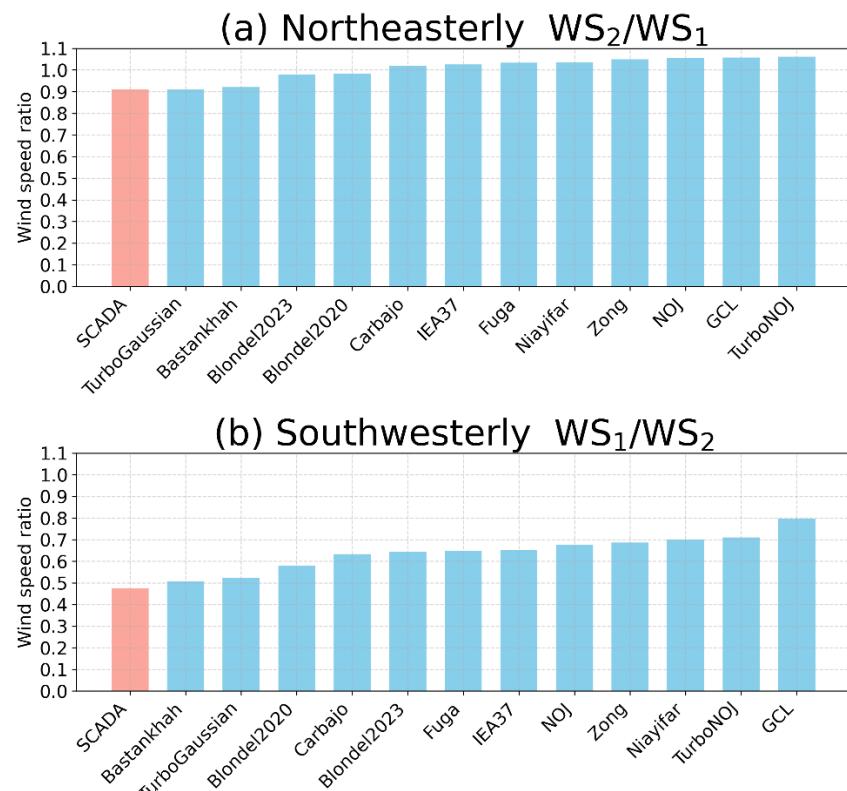
Figure 13. Wind speed ratio derived from the SCADA data and the wake models at wind direction with the maximum wake effects at wind speed of (a) 13 m s^{-1} for northeasterly wind and of (b) 8 m s^{-1} for southwesterly wind.

To investigate the different wake effects between northeasterly and southwesterly winds, we show vertical cross sections of horizontal wind speed computed by WAsP CFD and PyWake along the line connecting the two wind turbines (Figure 14). We computed wind flows with and without the effects of the wind turbines and derived the reduction in horizontal wind speed. In Figs. 14b and 14d, the TurboGaussian wake model is used. We can consider the path of the wake generated by the upstream wind turbine from the streamline passing through the center of the wind turbine wake (Sesarego et al., 2020). For northeasterly wind, the wind reaches the hub height of WT2 from the hub height of WT1 due to the wind ascending the hill (Fig. 14a). Moreover, the flow accelerates on the top of the hill around the location of WT2, and the accelerated wind blows through the rotor surface of WT2. When the wind turbines exist and are in operation, the Gaussian-shaped wake generated by WT1 rises slightly upward along the terrain and reaches the center of the rotor of WT2 (Fig. 14b). However, the wake weakens at WT2 because the flow accelerates on top of the hill. Thus, the wind speed ratios are generally higher than 1.0 due to the acceleration of wind speed over the hill in no-wake conditions (Fig. 7a) and the wind speed ratios slightly decrease due to the weakened wake and flow acceleration in wake conditions (Fig. 7b). For southwesterly wind, the weak winds in the lee of the hill of WT2 cover the location of WT1 and extend through the height of the lower part of the WT1 rotor (Fig. 14c). The flow separation is created by the hill where WT2 stands. In contrast, the strong winds on the top of the hill reach the hub height of WT1. The resulting strong vertical wind shear at the height of the rotor of WT1 contributes to the increase in turbulence. No acceleration occurs in the lee of the hill between WT1 and WT2. When the wind turbines exist and are in operation, the wake generated by WT2 extends horizontally through the upper part of the rotor of WT1 (Fig. 14d). The wake does not follow the terrain slope in the lee of the hill (Berg et al., 2017; Dar et al., 2019; Wenz et al., 2022). Thus, the wind speed ratios are generally lower than 1.0 due to weak winds in the lee of the hill in no-wake conditions (Fig. 7c). The wind speed ratios decrease significantly due to weak winds in the lee of the hill near the ground surface and due to the wake extending from the upstream wind turbine in wake conditions (Fig. 7d).
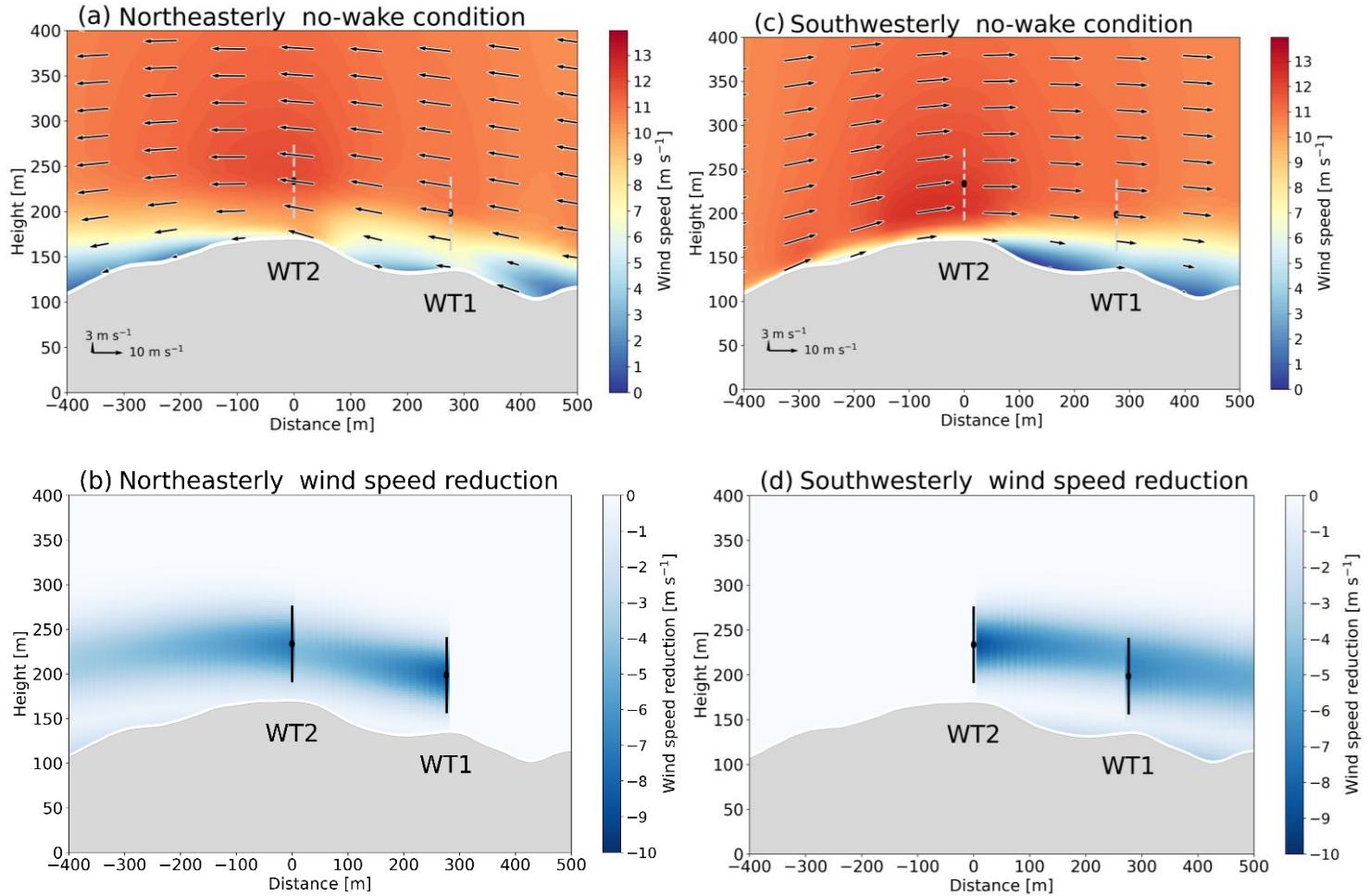
Figure 14. Vertical cross sections along the blue dashed line in Fig. 1 for (a) (b) northeasterly wind and (c) (d) southwesterly wind. In (a) and (c), we show horizontal wind speed (color shading) and wind vectors on the cross section with no wake effects of the wind turbines, although we show the positions of the rotors of the wind turbines by gray dashed line. In (b) and (d), we show a reduction in horizontal wind speed (color shading) due to the wind turbine wake. The black lines indicate the positions of the rotors of the wind turbines. The data from WAsP CFD are available from 5 m above ground level.

4 Summary and conclusions

We have investigated the bidirectional wake effects between the two wind turbines in complex terrain at a site in northern Japan using the SCADA data and validated the performance of the wake models. We have addressed the two issues: (1) to identify the wake effects generated by the upstream wind turbine for northeasterly and southwesterly winds in terms of reduction in wind speed, turbulence intensity, and power output at the downstream wind turbine. (2) to validate the performance of the wake models and impacts of the topography on the simulated wakes. The main results are summarized as follows.

(1) Using the SCADA data, we detected wake effects from the differences in the wind speed ratio between no-wake conditions and wake conditions. These conditions are classified by the operating state of the upstream wind turbine on the basis of the blade pitch angle. The upstream wind turbine in operating state reduces wind speed at the downstream wind turbine for both northeasterly and southwesterly winds. For northeasterly wind, the wind speed ratio in no-wake conditions generally exceeds 1.0 and the maximum reduction in wind speed due to the wake is 23%. For southwesterly wind, the wind speed ratio in no-wake conditions is generally below 1.0 and the maximum reduction in wind speed due to wake is 46%. Wake effects are enhanced more for

southwesterly wind than for northeasterly wind. Wake effects increase as inflow wind speed increase and reach maximum wake effects below the rated wind speed for both northeasterly and southwesterly winds. Turbulence intensity at the downstream wind turbine increases due to the wake generated by the upstream wind turbine for southwesterly wind, and the upper 10% data of turbulence intensity exceed the level of A+ category. The power output at the downstream wind turbine for southwesterly wind decreases more significantly than for northeasterly wind. From this investigation using the SCADA data, this study demonstrated that wake effects depend on the surrounding terrain and inflow wind speed. These results indicate the importance of considering the combined effects of wakes and topography.

(2) We compared the wind speed ratios derived from 12 wake models in PyWake with those from the SCADA data. The wind speed ratios derived from the wake models show strong dependence on speed of inflow wind. This dependence reflects the thrust curve used for wake computation in the wake models. The wake models commonly overestimate the reduction in wind speed for northeasterly wind and underestimate it for southwesterly wind. The wake models with high reproducibility are TurboGaussian and Bastankhah wake models. These models represent the minimum wind speed ratio or maximum reduction in wind speed close to the observations when inflow wind speeds are 13 m s^{-1} for northeasterly wind and 8 m s^{-1} for southwesterly wind. We can conclude that the topographic effects cause an opposite change in the simulated wakes compared to the SCADA data. The wake flow over the complex terrain computed by WAsP CFD and PyWake complemented the interpretation of the wind speed ratio results from the SCADA data. Then we examined wind filed by WAsP CFD. For northeasterly wind, the wake effects weaken at the downstream wind turbine dur to the acceleration of wind on the top of the hill. For southwesterly wind, wind speed at the downstream wind decreases significantly because of the weak winds in the lee of the hill and the wake extending horizontally to the down stream wind turbine from the upstream wind turbine.

By analysing the SCADA data, this study reveals the fundamental characteristics of bidirectional wake effects over complex terrain. The SCADA data have the potential to provide much information on wakes. The method used for detecting wake effects in this study demonstrates the potential to utilize the SCADA data collected during downtime of wind turbines due to maintenance and curtailment. Although this study focuses on onshore wind turbines, the findings provide important suggestions for offshore wind turbines near the coast influenced by terrain effects and for wind power plants subject to multiple wake interactions.

We further need to investigate the following aspects. First, examining impacts of atmospheric stability on wind turbine wakes is a challenge. In the study area, northeasterly wind dominates in summer and southwesterly wind dominates in winter (Sasanuma and Honda, 2020). That is, dominant winds and stability conditions might typically be fixed to the seasons. The following studies have investigated stability effects on wakes using numerical simulations (Uchida and Takakuwa, 2019; Yamaguchi et al., 2024) and observations (Oqaily, 2025). Uchida and Takakuwa (2019) show that the wind turbine wake on the top of the hill follows the terrain under stable atmospheric conditions, whereas, the wake rises on the lee side under neutral atmospheric stability conditions. Therefore, the magnitude of the wake effect depends not only on the terrain but also on the atmospheric stability. Then, increased turbulence intensity owing to wakes increases the risks of fatigue loads and shortens the lifespan of wind turbines. We have a next plan to evaluate quantitatively the fatigue loads, fatigue lifetime and power output at the downstream wind turbine by using aeroelastic simulation. The insight of risks on the downstream wind turbine will be valuable for the operating of wind power plant.

Appendix A: 12 wake models

We present 12 wake models used in this study in Table. A1.

460

Table A1. Abbreviations and full names for 12 wake models in PyWake.

Abbreviation	Full name	Reference
NOJ	NOJDeficit	Jensen, 1983
TurboNOJ	TurboNOJDeficit	Nygaard et al., 2020
Fuga	FugaDeficit	Ott et al., 2011
Bastankhah	BastankhahGaussianDeficit	Bastankhah and Porté-Agel, 2014
IEA37	IEA37SimpleBastankhahGaussianDeficit	Bastankhah and Porté-Agel, 2016
Niayifar	NiayifarGaussianDeficit	Niayifar and Porté-Agel, 2016
Zong	ZongGaussianDeficit	Zong and Porté-Agel, 2020
Carbajofuertes	CarbajofuertesGaussianDeficit	Carbajo et al., 2018
TurboGaussian	TurboGaussianDeficit	Nygaard et al., 2020
GCL	GCLDeficit	Larsen, 2009
Blondel2020	BlondelSuperGaussianDeficit2020	Blondel and Cathelain, 2020
Blondel2023	BlondelSuperGaussianDeficit2023	Blondel, 2023

Appendix B: Wind speed reduction using 12 wake models

465 We show the results of wind speed reduction using 12 wake models for northeasterly wind and southwesterly wind in Figs. B1 and B2. The horizontal axis indicates differences in wind direction with the minimum wind speed ratio at 0º for both the SCADA data and the results of the wake models. For northeasterly wind, several models underestimate the wind speed reduction (Figs. B1a, B1b, B1f, and B1j). For southwesterly wind, most of the models underestimate the wind speed reduction excluding Bastankhah wake model (Fig. B2d) and TurboGaussian wake model (Fig. B2i).
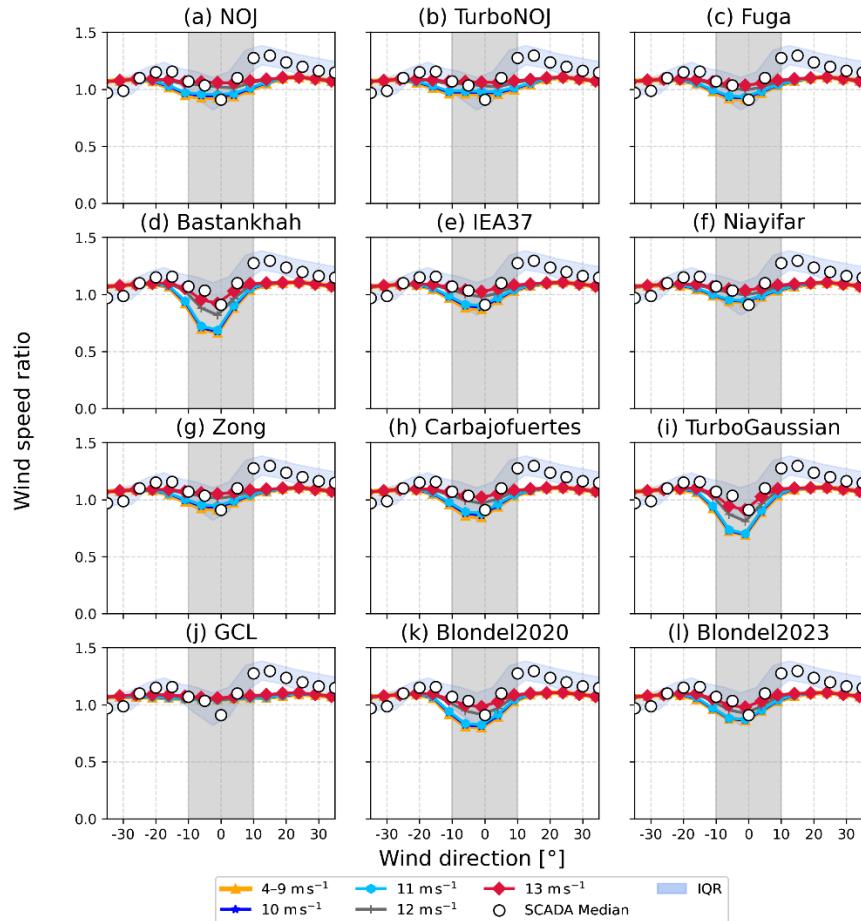
Figure B1. Wind speed ratio derived from 12 wake models for northeasterly wind. The blue band denotes the interquartile range (IQR) of the SCADA data and white circles denote median values in every 5º bin. Colored lines are results derived from each wake model for every 1 m s^{-1} for 4–13 m s^{-1}. The results for 4–9 m s^{-1} are shown by one line. Gray shading indicates the ranges of wind direction with wake effects.
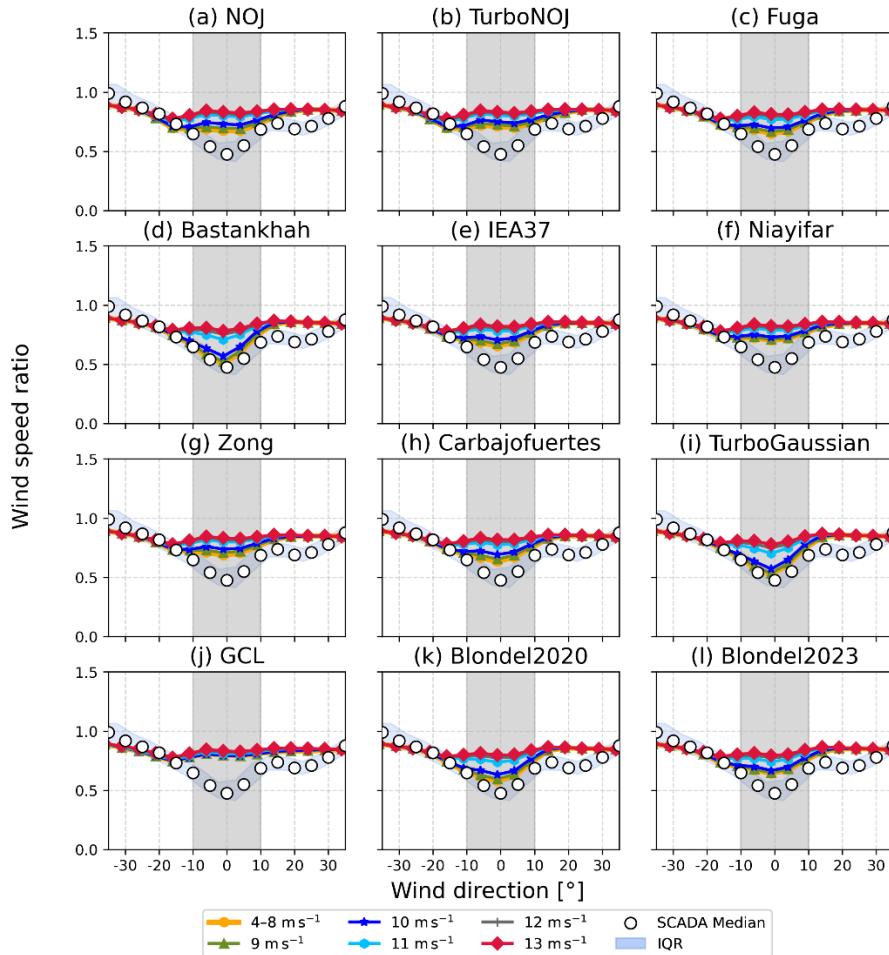
Figure B2. The same as in Fig. B1 but for southwesterly wind. The results for 4–8 m s⁻¹ are shown by one line.

480 **Code availability**

We used an open source in PyWake 2.5 (https://topfarm.pages.windenergy.dtu.dk/PyWake/ (last access: 17 July 2025)) and WAsP 12 (https://www.wasp.dk/software/wasp-cfd (last access: 17 July 2025)) in this study.

Data availability

485 The SCADA data were provided by Tsugaru Peninsula Eco Energy Co., Ltd. and were unavailable to the public.

Author contribution

Writing (original draft preparation) and visualization: NS, and TS. Writing (review and editing): NS, TS, AH, CB, NT, MG, and MN. Methodology and investigation: NS, AH, MG, and TS. Software: NS and MN. Conceptualization: NS, AH, and TS. All authors
490 contributed with critical feedback on this research and have read and agreed to the published version of the paper.

Competing interests

The authors declare that they have no competing interests.

Acknowledgments

First of all, we would like to thank the two anonymous reviewers and the editors for their comment on this paper. We would like
to express my gratitude to the staff of Tsugaru Peninsula Eco Energy Co., Ltd. and the staff of Japan Steel Works, Ltd. for providing
the observational data. We appreciate Mr. Mads Mølgaard Pedersen in analysing PyWake and Ms. Ginka Georgieva Yankova for
data uncertainty analysis. This research was supported by the JST Challenging Research Program for Next-Generation Researchers
JPMSP2152.

References

Astolfi, D., Castellani, F., and Terzi, L.: A study of wind turbine wakes in complex terrain through RANS simulation and SCADA
data, J. Sol. Energy Eng., 140, 031001, https://doi.org/10.1115/1.4039093, 2018.

Bastankhah, M., and Porté-Agel, F.: A new analytical model for wind-turbine wakes. Renewable Energy, 70, 116-123.
https://doi.org/10.1016/j.renene.2014.01.002, 2014.

Bastankhah, M., and Porté-Agel, F.: Experimental and theoretical study of wind turbines wakes in yawed conditions, Journal of
Fluid Mechanics, 806, 506-541, 10.1017/jfm.2016.595, 2016.

Bechmann, A., N. N. Sørensen, J. Berg, J. Mann, and Réthoré P.-E.: The Bolund Experiment, Part II: Blind Comparison of
Microscale Flow Models, Boundary-Layer Meteorology 141 (2): 245–71, https://doi.org/10.1007/s10546-011-9637-x, 2011.

Bechmann, A.: WAsP CFD A new beginning in wind resource assessment, Tech. rep., Risø National Laboratory, Denmark, 2012.

Bechmann, A.: Perdigão CFD Grid Study, DTU Wind Energy E 0120, 2016.

Berg, J., Troldborg, N., Sørensen, N.N., Patton E. G., and Sullivan, P. P.: Large-Eddy Simulation of turbine wake in complex terrain,
J. Phys.: Conf. Se. 854, 012003, 10.1088/1742-6596/854/1/012003, 2017.

Blondel, F. and Cathelain, M.: An alternative form of the super-Gaussian wind turbine wake model, Wind Energ. Sci., 5, 1225–
1236, https://doi.org/10.5194/wes-5-1225-2020, 2020.

Blondel, F.: Brief communication: A momentum-conserving superposition method applied to the super-Gaussian wind turbine wake
model, Wind Energ. Sci., 8, 141–147, https://doi.org/10.5194/wes-8-141-2023, 2023.

Carbajo Fuertes, F., and Markfort, C. D.: Wind Turbine Wake Characterization with Nacelle-Mounted Wind Lidars for Analytical
Wake Model Validation. Remote Sensing, 10, 668. https://doi.org/10.3390/rs10050668, 2018.

Castellani, F., Astolfi, D., Burlando, M., & Terzi, L.: Numerical modelling for wind farm operational assessment in complex terrain.
Journal of Wind Engineering and Industrial Aerodynamics, 147, 320-329. https://doi.org/10.1016/j.jweia.2015.07.016, 2015.

Centurelli, G., Dörenkämper, M., Bange, J., and Platis, A.: Evaluation of Engineering Models for large-scale cluster wakes with the
help of in situ airborne measurements. Wind Energy, 27(10), 1040-1062. https://doi.org/10.1002/we.2942, 2024.

Dar, A. S., Berg, J., Troldborg, N., and Patton, E. G.: On the self-similarity of wind turbine wakes in a complex terrain using large
eddy simulation, Wind Energ. Sci., 4, 633–644, https://doi.org/10.5194/wes-4-633-2019, 2019.

Dilip, D. and Porté-Agel, F.: Wind turbine wake mitigation through blade pitch offset, Energies, 10(6), 757,
https://doi.org/10.3390/en10060757, 2017.

Duncan Jr., J. B., Hirth, B. D., and Schroeder, J. L.: Exploring the complexities associated with full-scale wind plant wake mitigation
control experiments, Wind Energ. Sci., 5, 469–488, https://doi.org/10.5194/wes-5-469-2020, 2020.

El-Asha, S., Zhan, L., and Iungo, G. V.: Quantification of power losses due to wind turbine wake interaction through SCADA,
530   meteorological and wind LiDAR data, Wind Energy, 20, 1823–1839, https://doi.org/10.1002/we.2123, 2017.

Enomoto, S., Inomata, N., Yamada, T., Chiba, H., Tanikawa, R., Oota, T., and Fukuda, H.: Prediction of power output from wind
farm using local meteorological analysis, in: Proceedings of the European Wind Energy Conference, Copenhagen, Denmark, 2-5
June 2001, 749-752, ISBN 3-936338-09-4, 2001.

Farrell, A., King, J., Draxl, C., Mudafort, R., Hamilton, N., Bay, C. J., Fleming, P., and Simley, E.: Design and analysis of a wake
535   model for spatially heterogeneous flow, Wind Energ. Sci., 6, 737–758, https://doi.org/10.5194/wes-6-737-2021, 2021.

Fischereit, J., Schaldemose Hansen, K., Larsén, X. G., van der Laan, M. P., Réthoré, P.-E., and Murcia Leon, J. P.: Comparing and
validating intra-farm and farm-to-farm wakes across different mesoscale and high-resolution wake models, Wind Energ. Sci., 7,
1069–1091, https://doi.org/10.5194/wes-7-1069-2022, 2022.

Fleming, P., King, J., Dykes, K., Simley, E., Roadman, J., Scholbrock, A., Murphy, P., Lundquist, J. K., Moriarty, P., Fleming, K.,
540   van Dam, J., Bay, C., Mudafort, R., Lopez, H., Skopek, J., Scott, M., Ryan, B., Guernsey, C., and Brake, D.: Initial results from a
field campaign of wake steering applied at a commercial wind farm – Part 1, Wind Energ. Sci., 4, 273–285,
https://doi.org/10.5194/wes-4-273-2019, 2019.

Fleming, P., King, J., Simley, E., Roadman, J., Scholbrock, A., Murphy, P., Lundquist, J. K., Moriarty, P., Fleming, K., van Dam,
J., Bay, C., Mudafort, R., Jager, D., Skopek, J., Scott, M., Ryan, B., Guernsey, C., and Brake, D.: Continued results from a field
545   campaign of wake steering applied at a commercial wind farm – Part 2, Wind Energ. Sci., 5, 945–958, https://doi.org/10.5194/wes-
5-945-2020, 2020.

Fujikawa, T., Iwasaki, N., Suguro, Y., Iwanaga, Y., and Shibata, M.: Mitsubishi high efficiency large capacity wind turbines,
Mitsubishi heavy industries, Ltd. Technical review, 39, 101-106, https://www.researchgate.net/publication/237268778, 2002.

Geospatial Information Authority of Japan: https://maps.gsi.go.jp/, last access: 9 April 2025.

550   Göçmen, T., Laan, P. V. D., Réthoré, P., Diaz, A. P., Larsen, G. C., and Ott, S.: Wind turbine wake models developed at the technical
university of Denmark: A review. Renewable and Sustainable Energy Reviews, 60, 752-769.
https://doi.org/10.1016/j.rser.2016.01.113, 2016

Han, X., Liu, D., Xu, C., and Shen, W., Z.: Atmospheric stability and topography effects on wind turbine performance and wake
properties in complex terrain, Renewable Energy, 126, 640-651, https://doi.org/10.1016/j.renene.2018.03.048, 2018.

555   Hansen, K.S., Larsen, G.C., Menke, R., Vasiljevic, N., Angelou, N., Feng, J., Zhu, W.J., Vignaroli, A., Liu, W., Xu, C., and Shen,
W.Z.: Wind turbine wake measurement in complex terrain. J. Phys. Conf. Ser. 753, 1-10, https://doi.org/10.1088/1742-
6596/753/3/032013, 2016.

Hasegawa, Y., Kikuyama, K., Imamura, H., Inomata, N., Suzuki, H., and Ishikawa, H.: Fundamental study for estimation of wind
energy resources (Wind Measurements at Tappi Wind Park), Nihon kikai gakki ronbunshu, B Hen/Transactions of the Japan
560   Society of Mechanical Engineers, Part B, 69, 2052-2058, 10.1299/kikaib.69.2052, 2003.

IEC – International Electrotechnical Commission: IEC 61400-1: Wind energy generation systems – Part 1: Design requirements,
4th Edn., Geneva, Switzerland, 2019.

Inomata, N., Tsuchiya, K., and Yamada, S.: Measurement of stress on blade of NEDO's 500 kW prototype wind turbine, Renewable
Energy, 16, 912-915, https://doi.org/10.1016/S0960-1481(98)00309-7, 1999.

565   Jeon, S., Kim, B., and Huh, J.: Comparison and verification of wake models in an onshore wind farm considering single wake
condition of the 2 MW wind turbine. Energy, 93, 1769-1777. https://doi.org/10.1016/j.energy.2015.09.086, 2015.

Jensen, N., O.: A note on wind generator interaction, Risø National Laboratory; 1983.

Larsen, G. C.: A simple stationary semi-analytical wake model", Risø National Laboratory for Sustainable Energy, Technical
University of Denmark. Denmark. Forskningscenter Risoe. Risoe-R, No. 1713(EN), 2009.

570 Letzgus, P., Guma, G., and Lutz, T.: Computational fluid dynamics studies on wind turbine interactions with the turbulent local flow field influenced by complex topography and thermal stratification, Wind Energ. Sci., 7, 1551–1573, https://doi.org/10.5194/wes-7-1551-2022, 2022.

Mittelmeier, N., Allin, J., Blodau, T., Trabucchi, D., Steinfeld, G., Rott, A., and Kühn, M.: An analysis of offshore wind farm SCADA measurements to identify key parameters influencing the magnitude of wake effects, Wind Energ. Sci., 2, 477–490,
575 https://doi.org/10.5194/wes-2-477-2017, 2017.

Niayifar, A, and Porté-Agel, F.: Analytical Modeling of Wind Farms: A New Approach for Power Prediction. Energies, 9(9), 741. https://doi.org/10.3390/en9090741, 2016.

Nygaard, N., G., Steen, S., T., Poulsen, L., and Pedersen, J., G.: Modelling cluster wakes and wind farm blockage, J. Phys. Conf. Sr., 1618, 062072, 10.1088/1742-6596/1618/6/062072, 2020.

580 Oqaily, D. A., Giani, P., & Crippa, P.: Evaluating WRF Multiscale Wind Simulations in Complex Terrain: Insights from the Perdigão Field Campaign. Journal of Geophysical Research: Atmospheres, 130(15), e2025JD044055. https://doi.org/10.1029/2025JD044055, 2025.

Ott, S., Berg, J., and Nielsen, M.: Linearised CFD models for wakes. Technical report, Danmarks Tekniske Universitet, Risø Nationallaboratoriet for Bæredygtig Energi, Forskningscenter Risoe. Risoe-R No. 1772(EN), 2011.

585 Pedersen, J. G., Svensson, E., Poulsen, L., and Nygaard, N. G.: Turbulence Optimized Park model with Gaussian wake profile, J. Phys. Conf. Sr., 2265 022063, 10.1088/1742-6596/2265/2/022063, 2022.

Pedersen, M. M., van der Laan, P., Friis-Møller, M., Forsting, A. M., Riva, R., Romàn, L. A. A., Risco, J., C., Quick, J., Christiansen, J. P. S., Olsen B. T., Rodrigues, R. V., and Réthoré, P. E., DTU WindEnergy/PyWake: PyWake (v2.5.0), https://doi.org/10.5281/zenodo.6806136, 2023.

590 Politis, E. S., Prospathopoulos, J., Cabezon, D., Hansen, K. S., Chaviaropoulos, P. K., & Barthelmie, R. J.: Modeling wake effects in large wind farms in complex terrain: The problem, the methods and the issues. Wind Energy, 15(1), 161-182. https://doi.org/10.1002/we.481, 2011.

Porté-Agel, F., Bastankhah, M. & Shamsoddin, S.: Wind-Turbine and Wind-Farm Flows: A Review, Boundary-Layer Meteorol., 174, 1–59, https://doi.org/10.1007/s10546-019-00473-0, 2020.

595 Rhodes, M. E., and Lundquist, J. K.: The effect of wind-turbine wakes on summertime US midwest atmospheric wind profiles as observed with ground-based Doppler lider, 149, 85-103, https://doi.org/10.1007/s10546-013-9834-x, 2013.

Ruisi, R. and Bossanyi, E.: Engineering models for turbine wake velocity deficit and wake deflection. A new proposed approach for onshore and offshore applications, in: Journal of Physics: Conference Series, vol. 1222, p. 012004, IOP Publishing, 2019.

Sasanuma, N., Honda, A.: Wind analyzing of wind turbines and lighthouse in Tappi with relative point of view, Wind Engineering
600 Symposium, 26, 19-24, https://doi.org/10.14887/natsympwindengproc.26.0_19, 2020.

Sasanuma, N., and Honda, A.: Study on wind characteristic and wind wake effect in complex terrain, Journal of wind engineering, 27, 294-302, https://doi.org/10.14887/windengresearch.27.0_294, 2022.

Sasanuma, N., and Honda, A.: Observation survey on wind turines installed close to complex terrain: the effects terrain and wind tubine wake, Journal of wind engineering, 28, 267-275, https://doi.org/10.14887/windengresearch.28.0_267, 2024.

605 Sessarego, M., Feng, J., Friis-Møller, M., Xu, Y., Xu, M. and Shen, W., Z.: Development of a streamline wake model for wind farm perfomance predictions, J. Phys. Conf. Sr., 1618, 062027, 10.1088/1742-6596/1618/6/062027, 2020.

Sharma, P. K., Warudkar, V., & Ahmed, S.: Application of a new method to develop a CFD model to analyze wind characteristics for a complex terrain. Sustainable Energy Technologies and Assessments, 37, 100580. https://doi.org/10.1016/j.seta.2019.100580, 2020.

610 Shimada, T., Sawada, M. and Iwasaki, T.: Indices of cool summer climate in northern Japan: Yamase indices, J. Meteor. Soc. Japan, 92, 17-35, 10.2151/jmsj.2014-102, 2014.

Troen, I., and Hansen, B. O.: Wind Resource Estimation in Complex Terrain: Prediction Skill of Linear and Nonlinear Micro-Scale Models, Paper presented at AWEA Windpower Conference & Exhibition, Orlando Orange County Convention Center, United States. May 18, 2015.

615 Troldborg, N., Andersen, S. J., Hodgson, E. L., and Meyer Forsting, A.: Brief communication: How does complex terrain change the power curve of a wind turbine?, Wind Energ. Sci., 7, 1527–1532, https://doi.org/10.5194/wes-7-1527-2022, 2022.

Uchida, T., and Takakuwa, S.: Numerical Investigation of Stable Stratification Effects on Wind Resource Assessment in Complex Terrain. Energies, 13(24), 6638. https://doi.org/10.3390/en13246638, 2019.

Ushiyama, I.: Wind energy activities in Japan, Renewable Energy, 16, 811-816, https://doi.org/10.1016/S0960-1481(98)00261-4

620 1999, 1999.

Wagner, J., Gerz, T., Wildmann, N., and Gramitzky, K.: Long-term simulation of the boundary layer flow over the double-ridge site during the Perdigão 2017 field campaign, Atmos. Chem. Phys., 19, 1129–1146, https://doi.org/10.5194/acp-19-1129-2019, 2019.

Wenz, F., Langner, J., Lutz, T., and Krämer, E.: Impact of the wind field at the complex-terrain site Perdigão on the surface pressure

625 fluctuations of a wind turbine, Wind Energ. Sci., 7, 1321–1340, https://doi.org/10.5194/wes-7-1321-2022, 2022.

Yamaguchi, A., Ishihara, T., and Fujino, Y.: Applicability of linear and nonlinear wind prediction models to wind flow in complex terrain, in: Proceedings of The World Wind Energy Conference and Exhibition, Berlin, Germany, 3-8 July 2002, 1-4, https://www.researchgate.net/publication/266863617, 2002.

Yamaguchi, A., Tavana, A., and Ishihara, T.: Assessment of wind over complex terrain considering the effects of topography,

630 Atmospheric stability and turbine wakes, Atmosphere, 15, 723, https://www.mdpi.com/2073-4433/15/6/723, 2024.

Yang, X., Sotiropoulos, F., Conzemius, R. J., Wachtler, J. N., & Strong, M. B.: Large-eddy simulation of turbulent flow past wind turbines/farms: The Virtual Wind Simulator (VWiS). Wind Energy, 18(12), 2025-2045. https://doi.org/10.1002/we.1802, 2015.

Zong, H., and Porté-Agel, F.: A momentum-conserving wake superposition method for wind farm power prediction. Journal of Fluid Mechanics, 889:A8, 10.1017/jfm.2020.77, 2020.

635 zum, Berge, K., Centurelli, G., Dörenkämper, M., Bange, J., and Platis, A.: Evaluation of Engineering Models for large-scale cluster wakes with the help of in situ airborne measurements. Wind Energy, 27(10), 1040-1062. https://doi.org/10.1002/we.2942, 2024.